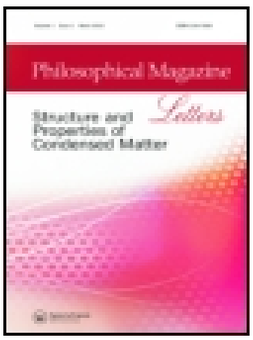

Philosophical Magazine Letters

ISSN: (Print) (Online) Journal homepage: https://www.tandfonline.com/loi/tphl20

Large deformability of Mg alloys produced by confinement to the nanoscale in one dimension

Shan Gong , Jörg M. K. Wiezorek & M. Ravi Shankar

To cite this article: Shan Gong , Jörg M. K. Wiezorek & M. Ravi Shankar (2020): Large deformability of Mg alloys produced by confinement to the nanoscale in one dimension, Philosophical Magazine Letters, DOI: 10.1080/09500839.2020.1783008

To link to this article: https://doi.org/10.1080/09500839.2020.1783008

Published online: 29 Jun 2020.

PHILOSOPHICAL MAGAZINE LETTERS
https://doi.org/10.1080/09500839.2020.1783008

Taylor & Francis
Taylor & Francis Group

Large deformability of Mg alloys produced by confinement to the nanoscale in one dimension

Shan Gong[a], Jörg M. K. Wiezorek[b] and M. Ravi Shankar[a,b]

[a]Department of Industrial Engineering, Swanson School of Engineering, University of Pittsburgh, Pittsburgh, PA, USA; [b]Department of Mechanical Engineering and Materials Science, Swanson School of Engineering, University of Pittsburgh, Pittsburgh, PA, USA

ABSTRACT

We report a transition to large-strain, multi-slip plasticity in Mg alloys resulting from refinement of a single dimension of the deformation geometry to the ~ 100 nm-scale. Basal-slip-dominated strain localisation and fracture is suppressed and shear strains greater than 200% are realised at ambient temperatures when one characteristic dimension is refined in an asymmetric wedge indentation, even when the other two dimensions remain macroscopic. The ductility at sub-critical scales of low dimensionality discovered here is independent of crystal orientation, and interfaces and large shear strains result in homogeneous nanocrystallinity in the deformed material under these conditions.

ARTICLE HISTORY
Received 17 June 2019
Accepted 9 June 2020

KEYWORDS
Magnesium alloys; severe plastic deformation; nanocrystalline microstructure

1. Introduction

The uniaxial symmetry of Mg, which has a hexagonal close-packed crystal structure, results in large anisotropy for the critical resolved shear stress (CRSS) of the basal slip (easy, with low CRSS) and non-basal slips (hard, with high CRSS). For general plasticity of arbitrary and multiaxial strains, the activation of non-basal slip, i.e. prismatic and/or pyramidal slip, is required. However, this is stymied by the high CRSS for non-basal slip [1,2]. Although deformation twinning offers an additional pathway, it is a polar mechanism, which is highly orientation specific and in which the magnitude of the accommodated plastic strain is limited [3]. These inherent constraints in Mg have motivated efforts aimed at alloy design to encourage non-basal slip and/or weakening basal texture formation [4–6], microstructure engineering to augment the role of grain-boundary-mediated plasticity [7–9], and nanoparticle-reinforced composite designs to optimise the balance of strength and ductility [10,11].

CONTACT M. Ravi Shankar ravishm@pitt.edu Department of Industrial Engineering, Department of Mechanical Engineering and Materials Science, Swanson School of Engineering, University of Pittsburgh, 3700 O'Hara Street, Pittsburgh, PA 15261, USA

Supplemental data for this article can be accessed https://doi.org/10.1080/09500839.2020.1783008

Plastic deformation is strongly length-scale dependent. Uniaxial deformation of micro/nano-scale Mg test-specimens reveals that (a) smaller is stronger, (b) twinning is difficult in small volumes and (c) non-basal slip becomes easier [12–15]. Exploring discrete combinations of loading axis with respect to the sample's crystal orientation, (e.g. $[11\bar{2}0]$ [12], [0001], see [13,14]) has revealed the ability to accommodate up to around tens of percent in plastic strain.

Here, we show that Mg alloys can deform to large shear strains, larger than 2, without the onset of shear localisation or fracture under ambient temperature conditions when just one characteristic dimension of the deformation geometry is reduced to be in the nanoscale ($\sim$ 100 nm). The other dimensions can be orders-of-magnitude larger or even macroscopic. By introducing plane-strain asymmetric wedge-indentation, which mimics plane-strain machining at micro/nanometre-scales as a test of material response, we demonstrate quasi-static accommodation of large (simple) shear strains in Mg alloys. Plastic-deformation-driven multiplication and reorganisation of dislocation structures results in characteristic microstructure refinement, which is normally associated with nominally ductile highly formable metals, which typically have isometric (cubic) crystal structures. Furthermore, this phenomenon is shown to be independent of the crystal orientation with respect to the applied deformation, which points to a broader motif for triggering a transition in the underlying mechanisms of plastic strain accommodation.

2. Experiments and results

The plane-strain deformation configuration is illustrated in Figure 1A, where a single-crystal diamond wedge (indenting tool) is advanced against a sample with the characteristic length scale of deformation defined by the pre-set depth a_0. The edge radius of the single-crystal diamond indenting tool is $\leq$ 25 nm. The sample material examined here is commercially available Mg AZ31 alloy. Figure 1B illustrates the microcrystalline structure of a bulk AZ31 sheet, several mm long and $\sim$ 300 μm wide (w in Figure 1A). The orientations of the individual grains and the direction of the nominal shear (white arrows in Figure 1A) are not typically aligned to favour basal slip. The observations in this work are, therefore, not an artefact of any preferential alignment that happens to accommodate the large strains. Choosing $a_0 \ll w$ ensures plane-strain deformation [16]. The experiments were performed on a deformation stage inside an SEM (see SI and Figure S1), which probe a_0 from $\sim$ 100 nm to $\sim$ 10 μm. The choice of this platform allows for selectively refining one characteristic length scale (a_0) of the deformation geometry, while simultaneously allowing for the imposition of simple shear strains with *in situ* observation of material flow, as seen in Figure 1A [17]. The experiments impose plane-strain deformation within a pre-set a_0, which is much smaller than the average grain size of the starting material ($\sim$ 30μm). In such configuration, an undeformed bulk volume characterised by a length L and

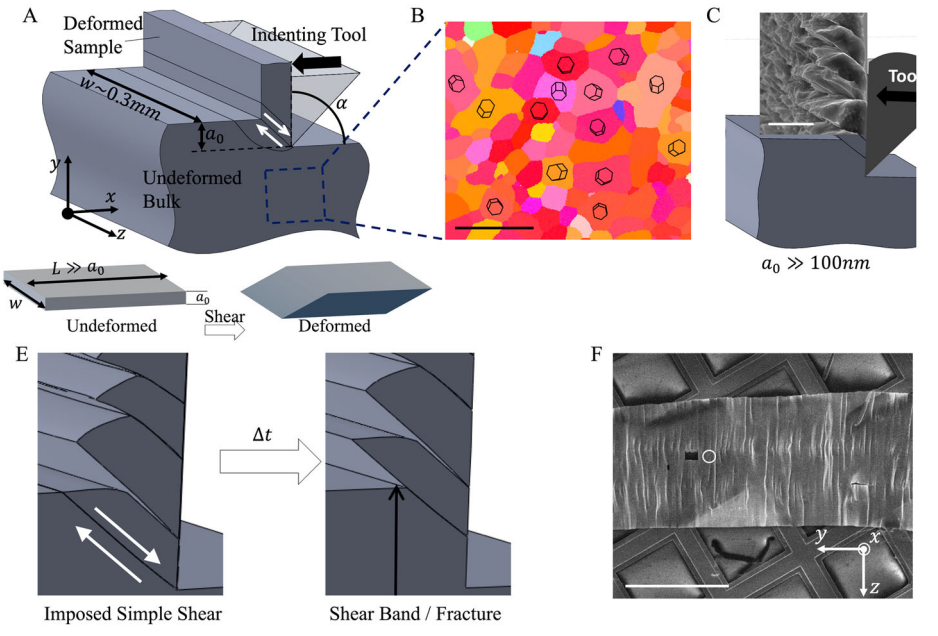

Figure 1. (A) Illustration of the asymmetric-wedge indentation process. *z* direction corresponds to the normal direction of the bulk microcrystalline sheet, which is used in the experiments. Inset: Illustrating geometry change from undeformed to deformed state. (B) Orientation map of bulk Mg AZ31 from electron backscatter diffraction, illustrating a characteristic basal texture. Note that the shear deformation is imposed in a manner that is not aligned with the basal slip in the majority of the grains. Schematic representation of distinct deformation regimes at two different length scales, which are overlaid with SEM micrographs of the deformed material: (C) $a_0 \gg$100 nm, and (D) $a_0 \sim$100 nm. Figure S3 illustrates the uncropped images of the deformed material corresponding to C and D. (E) Illustration of intermittent fracture leading to the serrated geometry of the deformed material, where segments of modestly deformed material are bound by shear bands. (F) Micrograph of a plastically deformed material with $a_0 = 150$ nm and $V = 150$ µm/s. The sample is macroscopic along the *y* and *z* axes. (G) Bright-field transmission electron micrograph of the plastically deformed material in F. The location of the image is identified with a white circle in F. Inset: Selected-area electron diffraction pattern.

width w, both of which are $\gg a_0$, is converted into a deformed 'chip' via simple shear as in the inset of Figure 1A. Refining the characteristic thickness a_0 of the deformation geometry will subsequently be shown to result in a transition in the deformation behaviour, which is not only independent of the orientation of shear with respect to the crystal axis (when essentially sampling one grain at a time) but also with respect to constraints imposed by the requirement of compatibility between neighbouring grains.

In the experiments, the angle of the wedge α is held constant at 90° as shown in Figure 1A. If the material can accommodate the imposed strains fully via plastic deformation ahead of the diamond tip, the shear strain is [16]:

$$\varepsilon = \cot\varphi + \tan\varphi > 2 \tag{1}$$

where φ is calculated from $\tan\varphi = a_0/a_c$, where a_c is the thickness of the material that was plastically deformed to create a 'chip' from a prior undeformed depth a_0. Usually, $a_c > a_0$. The strains are imposed in a shear deformation zone ahead of the tool tip, which transforms the undeformed bulk into the severe plastically deformed material. The diamond tool is advanced into the sample at a speed of $V = 150$ μm/s. The temperature rise in the deformation zone associated with accumulation of plastic strain caused by the work done by the indenting tool is given by

$$\rho C_p \Delta T = (1-\beta)\tau\varepsilon \tag{2}$$

where $\rho = 1.8\ \mathrm{g/cm^3}$ is the density and $C_p = 1.0059$ J/gK is the specific heat capacity of Mg AZ31 [18]. The shear strength is 50% of the tensile strength τ(=145 MPa) and the shear strain is $\varepsilon \sim 2.6$. β is the fraction of the heat dissipated in the bulk material, given by $\beta = \frac{1}{\alpha}\mathrm{erf}\sqrt{\alpha} + (1+\alpha)\,\mathrm{erfc}\sqrt{\alpha} - \frac{e^{-\alpha}}{\sqrt{\pi}}\left(\frac{1}{2\sqrt{\alpha}} + \sqrt{\alpha}\right) \sim 0.9993$, with $\alpha = \frac{1}{4}(Va_0\tan\varphi)\kappa$. The thermal diffusivity $\kappa = 4.8697 \times 10^{-5}\ \mathrm{m^2/s}$ [18]. We find that the temperature increase is no more than a few Kelvins in the shear zone. Even though the strains are large, the rate of deformation is small. The role of frictional heating is negligible since the friction coefficient at the diamond surface is characteristically small (~ 0.1) [19] and diamond has a high thermal conductivity [20]. This is an intended consequence of our choice of a_0, which minimises the thermomechanical-coupled temperature rise.

The inset SEM micrographs in Figure 1C and D illustrate the morphologies of the deformed material. When $a_0 \gg 100$ nm, advancing the tool into the sample attempts to impose shear deformation in an element of the material as illustrated in Figure 1E. However, this element fails to accommodate large strains, and instead fractures occur. Plastic deformation plays only a small role in creating the segmented and serrated deformed material [16]. This is a manifestation of the characteristic shear banding in Mg alloys, which is operative at the macro- and micro-metre length scales. Note that Equation 1 for large strain deformation via simple shear is not applicable in the case of fracture if the material fails to accommodate the strains via plastic deformation. The intermittency in the deformation can be understood as follows (see Figure 1E): an element of material is pushed into the deformation zone, where strains are progressively accumulated. While some plastic deformation can be accommodated, the progressive imposition of strains leads to fracture within shear bands. The fractured material displaces along the surface of the indenting tool and a new element of material advances into the deformation zone to continue this cycle (see Movie S1). This is a characteristic feature in Mg AZ31 when the deformation geometry involves supercritical (micro/meso-macroscopic) length scales.

However, reducing a_0 into the $\sim$ 100 nm regime indicates a transition in the deformation response as seen in the morphology of the deformed material in Figure 1D. In this particular experiment $a_0 = 150$ nm. The saw-tooth deformation is replaced with the characteristic 'sinuous flow', typically associated with highly ductile and formable materials [21]. The imposed shear strain is $\sim$ 2.6 using Equation 1. To provide a frame of reference, Figure S2 illustrates the morphology of a severely plastically deformed Cu sample deformed under conditions similar to that used in AZ31. The phenomenon of sinuous flow during an otherwise large strain plastic deformation is a characteristic feature of machining-based deformation configurations, where a geometric boundary condition is not explicitly enforced on the free surface of the deformed material.

While the transition observed for the morphology of the deformed material yields circumstantial evidence, it is not sufficient to conclude that severe plastic deformation occurred. To examine the deformed material for the presence of the characteristic microstructural attributes of severe plastic deformation, sections were extracted and placed on a Cu-grid as in Figure 1F. The sections were sufficiently thin, and reasonably transparent to the electron beam without any additional preparation steps, to allow direct imaging by TEM, which did not reveal any intermittently cracked or inhomogeneously deformed material. It should be recalled that, while $a_0 \ll$ grain size, the deformed material is essentially macroscopic along the z-axis, where the deformation samples multiple grains (albeit individually deformed in plane-strain). Attention should be paid to the rigid rotation of 90° from a_0 to deformed material owing to the geometry of simple shear deformation.

The refinement in Figure 1G from an otherwise microcrystalline bulk is commonly observed when a material is subjected to severe plastic deformation. However, Mg AZ31 is not known to undergo such deformation at ambient temperature. It is also noteworthy that the dimension of the deformed sample shown in Figure 1F is at the 100 nm scale only through its thickness; the length and width are macroscopic and the nanocrystalline deformed structure originates from a multitude of parent grains. Refinement of just one characteristic length, a_0, of the deformation results in the dramatic transition in the characteristic deformation behaviour. Therefore, this behaviour is likely to be independent of the underlying orientations of the individual grains in the undeformed parent material. Indeed, $a_0 = 150$ nm is much smaller than the typical grain size of the parent material ($\sim$ 30 μm). However, the large lateral width and length dimensions of the deformed material volumes reveal that, irrespective of the parent grain orientations, Mg AZ31 can undergo intergranular-compatible plastic deformation to large shear strains under ambient conditions to create an integral deformed sample (Figure 1F).

The bright-field images of cross-sections from the deformed samples are shown for $a_0 = 2$ μm in Figure 2A and $a_0 = 150$ nm in Figure 2C, which mirror the morphologies illustrated in Figure 1C and D, respectively. The

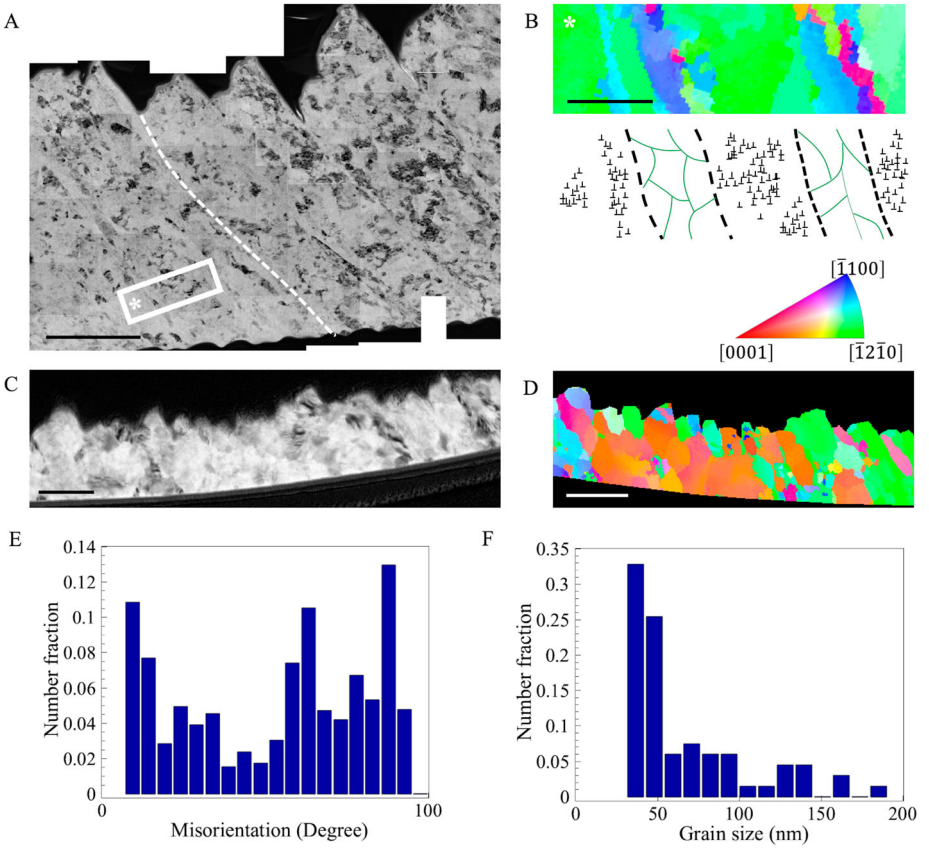

Figure 2. (A) Bright-field image of cross section of deformed material from AZ31 produced with $a_0 = 2$ µm. The dashed white line is a guide for the eye showing the location of a shear band. (B) Orientation map of a selected area in A (indicated with a white rectangle) and a schematised illustration of shear banded microstructure. (C) Bright-field image of cross section of deformed material with $a_0 = 150$ nm. Also see Figure S4. (D) Orientation map of selected area in (C) obtained vis TEM OIM. (E) Kernel average misorientation map corresponding to (D). (F) Crystallographic misorientation distribution ($\geq 5°$) and (G) grain size distribution (for crystallites separated by boundaries with misorientation $\geq 15°$) corresponding to conditions in (D). Refer to the colour triangle below (D) for orientation encoding in (B) and (D). Velocity of diamond tip $V =$ 150 µm/s.

segmented, deformed geometry clearly shows that the Mg AZ31 alloy undergoes shear banding at length scales $\gtrsim$2 µm. Figure 2A illustrates an intermittently plastically deformed material, where discrete segments of the material are separated by shear bands (one is illustrated by a dashed white line in Figure 2A). Fracture occurs in the shear bands to create the saw-toothed morphology in Figure 1C. Owing to an insufficient number of available slip systems, the deformation of each discrete segment is mainly accommodated via basal slip and/or twinning (if possible) [22]. Only a limited accommodation of plastic strain occurs, which results in a coarse sub-grain structure in segments bounded by shear bands (Figure 2A). This microstructure inhomogeneity is illustrated in Figure 2B.

In contrast, the deformed material with $a_0 = 150$ nm features a uniformly nanocrystalline structure as illustrated in Figure 2C, which does not show the inhomogeneity observed at the larger length scale as illustrated in Figure 2D. The TEM micrographs in Figure 1F and 2C reveal an integral sample with no evidence of fracture or cracking, which reinforces the idea that the material accommodates the severe plastic strains. Also, see Figure S4 for a larger micrograph of the deformed material produced with $a_0 = 150$ nm, which illustrates a sample devoid of the characteristic microstructural inhomogeneity observed at the larger length scale (e.g. Figure 2A). Figure 2E confirms a significant portion of the grain boundaries in the deformed material having a large misorientation, with the grain size skewed to the sub-100 nm scale as shown in Figure 2F. We have not found any signs of deformation twinning, which is consistent with the expectation that dislocation plasticity plays a major role in accommodating large plastic strains in Mg at refined length scales [23]. While, these deformations conditions (i.e. the combination of the size-scale and strain rates at ambient conditions) do not appear to favour twinning, it is possible to envision analogous deformation conditions, albeit at sub-ambient (or cryogenic) temperatures, where twinning and slip can become mutually competitive [24].

A partially detached specimen contains the trajectory of the microstructure evolution from the bulk to the severely deformed material, across the deformation zone, as shown in Figure 3A and B. Given the grain size of bulk Mg AZ31, the deformation configuration essentially samples a small volume within a single grain in a given increment of time. The orientation of the undeformed material is not favourable for basal slip to accommodate the imposed shear (see inset in Figure 3B). Nevertheless, the deformation results in a nanocrystalline structure in the deformed material. The dislocation sub-structures, including incidental dislocation boundaries (IDBs), owing to statistical storage of dislocations, and geometrically necessary boundaries (GNBs), accommodating crystal lattice bending caused by strain gradient in plastic deformation [25], increase their mean misorientations gradually with progressive shear deformation, developing high-angle boundaries. This is illustrated in the plot in Figure 3C, which tracks the evolution of the misorientations from the parent undeformed grain in the bulk to deformed material along the arrow in Figure 3B.

Figure 3D illustrates an experiment where the deformation traverses a grain boundary. Two grains, whose orientations are schematised in the insets are shown to deform plastically up to large strains, while also retaining compatibility. This provides direct evidence for the transition in the deformation behaviour of Mg alloys being essentially independent of the grain structure. The continuity of shear is maintained across the boundary, presumably by activating additional slip systems for maintaining compatibility with the large shear strains [26]. In Figure 3D the grain boundary is illustrated using two white arrows in the deformed material, which mark the putative location of the boundary in the undeformed state.

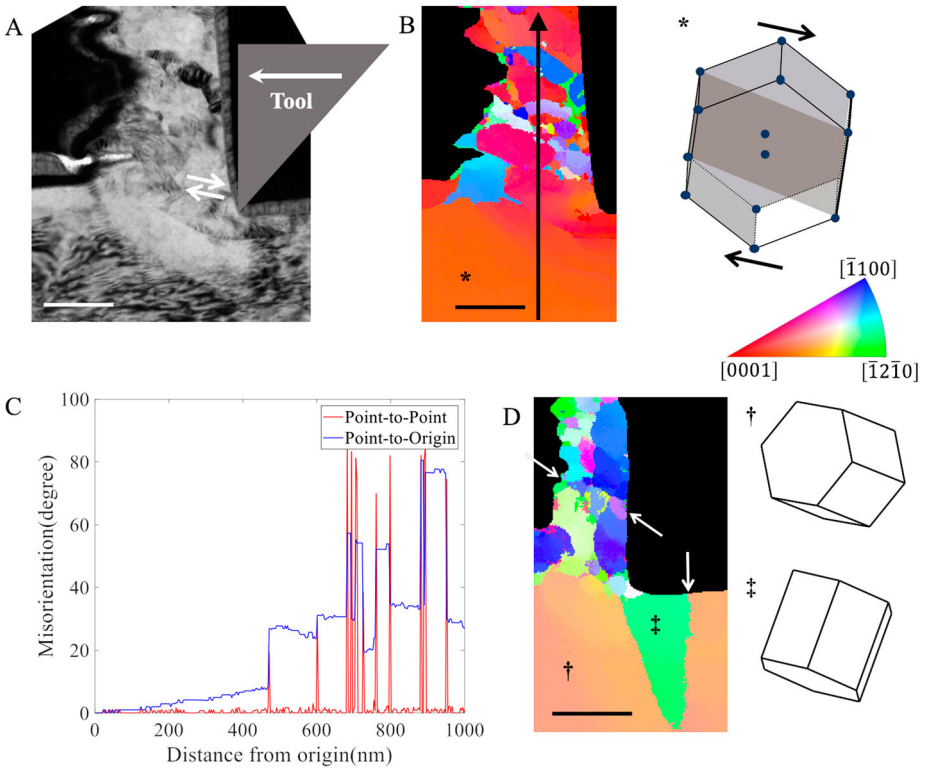

Figure 3. (A) Bright-field image of partially detached specimen from Mg AZ31. The nominal shear direction is illustrated by two white arrows. (B) Orientation map corresponding to the deformation zone in A. Crystal orientation and the shear direction are shown in inset. (C) Point-to-point and point-to-origin misorientation along the arrow in B illustrates the progressive evolution of a nanocrystalline grain structure via the imposition of severe shear deformation. (D) Orientation map of a partially detached specimen when deforming across to a grain boundary is shown. The pair of white arrows in the deformed material indicate the location of the boundary, which is indicated on the undeformed bulk. Orientation of the neighbouring undeformed grains is shown in inset. a_0 = 150 nm and V = 150 μm/s.

3. Discussion

The poor formability of Mg alloys at room temperatures has been attributed to the preponderance of basal slip vs. non-basal systems, with twinning offering modest supplementary strain accommodation. Notable exceptions arise only in specially oriented magnesium single crystals, where twinning and subsequent dynamic recrystallization can aid accommodation of large strains [27]. For this, it has been argued that the formation of 'shear cracks' result from strain localisation in shear bands in bulk Mg alloys when twinning and basal slip are both depleted as strain accommodation mechanisms [28]. Here, we find that refining only a_0 (as shown in Figure 1A) triggers a deformation behaviour that is dominated by multi-slip and engenders microstructure refinement, which is otherwise associated with highly formable metals. The diminution of

the role of twinning and dominance of dislocation multi-slip has been recognised at small length scales [23], though our experiments reveal that the dimensionality dictating this transition is 1 and not 3 (i.e. the entire sample volume).

In prior work on an analogous deformation experiments, albeit at macroscopic length scales, it has been shown that Mg AZ31 demonstrates prolific twinning and the deformed material is characteristically shear localised [29]. In Figures 3 and 4 we see no evidence of twinning in the deformation zone. Thus, with shrinking characteristic length scale of the deformation geometry when $a_0 \sim 100$ nm, twinning – which is a critical precursor for shear banding – is suppressed.

The progressive grain refinement during deformation under ambient conditions (as shown in Figure 3) arises from the tangling of dislocations along primary and secondary slip planes. The storage and rearrangement of dislocations result in cell structures and develop into subgrain and/or grain boundaries with progressing straining [30]. Multi-slip is central to generating the ultrafine microstructures from severe plastic deformation. When multi-slip becomes possible at sub-critical scales of a_0, grain refinement is observed (Figure 3), while segmented microstructures are observed at larger length scales (Figure 2A). Note that when grain refinement occurs at small values of a_0, there is a possibility that deformation can be accommodated via grain boundary sliding and rotation [31]. The role of these phenomena is uncertain.

The question then remains – how are multiple slip systems being activated at the nanoscale to accommodate the severe shear strains? The ratio of critical shear stresses for activating basal (τ^b_{CRSS}) vs., say, prismatic (τ^p_{CRSS}) slips in Mg

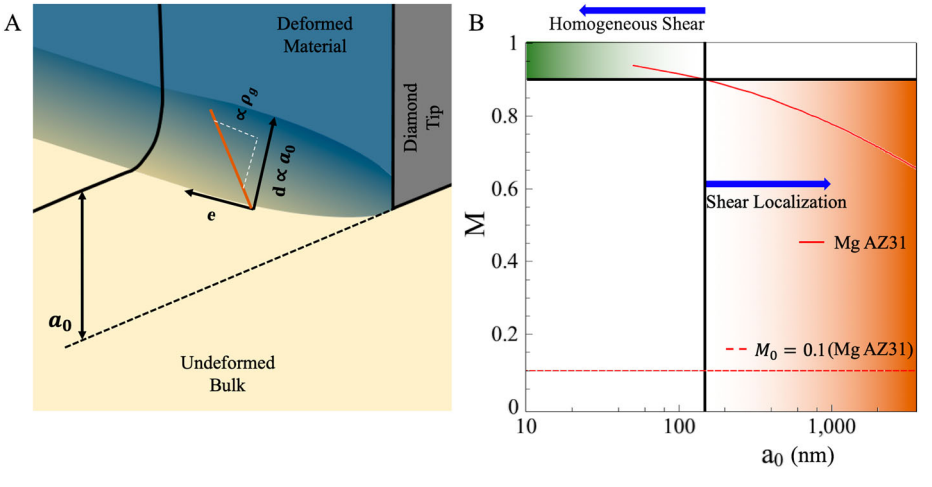

Figure 4. (A) Schematic of strain gradients in the deformation zone of asymmetric wedge indentation. (B) Mismatch factor M as a function of a_0. When a_0 is below $\sim$ 150 nm, $M > 0.9$. Thus, activation of multiple slip systems becomes easier and homogeneous accommodation of severe shear strains becomes feasible. When $a_0 \gg 100$ nm, intermittent plastic deformation involving shear localisation and fracture is the characteristic feature.

alloys, i.e. $M_0 = \tau^b_{\mathrm{CRSS}}/\tau^p_{\mathrm{CRSS}}$ is typically in the range $\sim 10^{-1}$ to 10^{-2} [2]. This mismatch M_0 is at the root of the poor formability. However, confining a_0 also leads to a magnification of the strain gradients in the deformation zone. It is clear from Figure 3C that the microstructure evolution is progressive through the deformation zone, where severe shear strains are imposed. The extent of the deformation zone δ is essentially proportional to a_0 (Figure 4A) and, as such, the geometrically necessary dislocation density caused by the strain gradient ρ_g scales as $\rho_g \sim 1/(ba_0)$ [32], where b is the Burgers vector = 0.32 nm. The strain gradient in the deformation zone shown in Figure 4A, leads to a continuous generation of geometrically necessary dislocations [32]. In addition, the large strains cause the accumulation of statistically stored dislocations. The geometrically necessary dislocation density leads to a strain-gradient-induced hardening of slip, which modifies the critical threshold for inducing slip on both basal and non-basal slip systems. Thus, the mismatch M for activating basal vs. say, prismatic slip is:

$$M = \frac{\tau^b_{CRSS} + \alpha b \mu \sqrt{\rho_g}}{\tau^p_{CRSS} + \alpha b \mu \sqrt{\rho_g}} \tag{3}$$

where $\mu = 17$ GPa, $\alpha \sim 1$. For AZ31, $\tau^b_{CRSS} \sim 10$ MPa and $\tau^p_{CRSS} \sim 100$ MPa. For the scaling arguments we employ here, this is roughly the order-of-magnitude observed in prior experiments [33]. Figure 4B illustrates M as a function of a_0, which illustrates how strain-gradient effects can reduce the mismatch when a_0 decreases. In particular, we find that when $a_0 \sim$150 nm, the mismatch $M \sim 0.9$. Thus, refining a_0 enables accommodation of large plastic strains via multi-slip, while engendering the characteristically dramatic microstructure refinement. This underpins a transition from shear-banding/fracture behaviour to one characterised by homogeneous deformation.

4. Conclusions

Refining one characteristic length scale of the deformation geometry to the 100 nm scale in an asymmetric wedge-indentation configuration leads to a transition in the deformation mechanics of Mg alloys under ambient temperature conditions, even when the other dimensions are essentially macroscopic. The characteristic shear banding and fracture is suppressed and severe plastic deformation to strains greater than 2 ensues, which leads to microstructural refinement in a manner that is otherwise observed in nominally formable metals. While the suppression of twinning under these conditions eliminates a critical precursor to the localisation of strains in shear bands, the magnified strain gradients offer a pathway for reducing the mismatch in the critical shear stresses required for activating basal and non-basal slip systems. The ability of Mg to accommodate shear strains greater than 200% in this configuration is

independent of the orientation of the crystals with respect to the loading direction. The strain gradients in the principal shear direction along with the spatial confinement hold the key to improving the ductility. This implies that achieving the combination of low density, high strength and formability in bulk Mg can be accomplished by designing microstructures and composites in fewer than 3D without requiring precise control over the crystal structure or orientation. For instance, creating laminate structures with characteristic thickness in the 100-nm scale can manifest the large strain deformability observed here, without resorting to any other microstructural engineering or composition design.

Acknowledgements

This work was supported by Block Gift Grant program of the II-VI foundation and National Science Foundation under grant number 1635926.

Disclosure statement

No potential conflict of interest was reported by the author(s).

Funding

This work was supported by Block Gift Grant program of the II-VI foundation and National Science Foundation under grant number 1635926.

References

[1] D.Y. Sun, M.I. Mendelev, C.A. Becker, K. Kudin, T. Haxhimali, M. Asta, et al., Phys. Rev. B 73 (2006) pp.1–12.
[2] W.B. Hutchinson and M.R. Barnett, Scr. Mater. 63 (2010) pp.737–740.
[3] J.J. Jonas, S. Mu, T. Al-Samman, G. Gottstein, L. Jiang and E. Martin, Acta Mater. 59 (2011) pp.2046–2056.
[4] J. Hirsch and T. Al-Samman, Acta Mater. 61 (2013) pp.818–843.
[5] D. Wu, R.S. Chen and E.H. Han, J. Alloys Compd. 509 (2011) pp.2856–2863.
[6] B.P. Zhang, L. Geng, L.J. Huang, X.X. Zhang and C.C. Dong, Scr. Mater. 63 (2010) pp.1024–1027.
[7] R.B. Figueiredo, S. Sabbaghianrad, A. Giwa, J.R. Greer and T.G. Langdon, Acta Mater. 122 (2017) pp.322–331.
[8] Z. Zeng, J.-F. Nie, S.-W. Xu, C.H.J. Davies and N. Birbilis, Nat. Commun. 8 (2017) p.972.
[9] C.M. Cepeda-Jiménez, J.M. Molina-Aldareguia and M.T. Pérez-Prado, Acta Mater. 84 (2015) pp.443–456.
[10] N. Stanford and M.R. Barnett, Mater. Sci. Eng. A 516 (2009) pp.226–234.
[11] L.Y. Chen, J.Q. Xu, H. Choi, M. Pozuelo, X. Ma, S. Bhowmick, et al., Nature 528 (2015) pp.539–543.
[12] G.S. Kim, S. Yi, Y. Huang and E. Lilleodden, Mater. Res. Soc. Symp. Proc. 1224 (2010) pp.9–14.

[13] C.M. Byer, B. Li, B. Cao and K.T. Ramesh, Scr. Mater. 62 (2010) pp.536–539.
[14] E. Lilleodden, Scr. Mater. 62 (2010) pp.532–535.
[15] Q. Yu, L. Qi, R.K. Mishra, J. Li and A.M. Minor, Proc. Natl. Acad. Sci. U. S. A. 110 (2013) pp.13289–13293.
[16] M.C. Shaw and J. Cookson, *Metal Cutting Principles*, Oxford university press, New York, 2005.
[17] S. Basu and M.R. Shankar, Acta Mater. 79 (2014) pp.146–158.
[18] S. Lee, H.J. Ham, S.Y. Kwon, S.W. Kim and C.M. Suh, Int. J. Thermophys. 34 (2013) pp.2343–2350.
[19] I.P. Hayward, Surf. Coatings Technol. 49 (1991) pp.554–559.
[20] L.S. Pan and D.R. Kania, *Diamond: Electronic Properties and Applications*, Springer Science & Business Media, New York, 2013.
[21] H. Yeung, K. Viswanathan, W.D. Compton and S. Chandrasekar, Proc. Natl. Acad. Sci. 112 (2015) pp.9828–9832.
[22] S. Sandlöbes, S. Zaefferer, I. Schestakow, S. Yi and R. Gonzalez-Martinez, Acta Mater. 59 (2011) pp.429–439.
[23] Q. Yu, Z.W. Shan, J. Li, X. Huang, L. Xiao, J. Sun, et al., Nature 463 (2010) pp.335–338.
[24] M.A. Meyers, O. Vöhringer and V.A. Lubarda, Acta Mater. 49 (2001) pp.4025–4039.
[25] D.A. Hughes and N. Hansen, Acta Mater. 48 (2000) pp.2985–3004.
[26] R.C. Pond, W.A.T. Clark and R.H. Wagoner, Scr. Metall. 20 (1986) pp.1291–1295.
[27] K.D. Molodov, T. Al-Samman, D.A. Molodov and G. Gottstein, Acta Mater. 76 (2014) pp.314–330.
[28] T. Al-Samman and G. Gottstein, Mater. Sci. Eng. A 488 (2008) pp.406–414.
[29] S. Basu, S. Abolghasem and M.R. Shankar, Metall. Mater. Trans. A Phys. Metall. Mater. Sci. 44 (2013) pp.4558–4566.
[30] J.W. Steeds, Proc. R. Soc. London. Ser. A. Math. Phys. Sci. 292 (1966) pp.343–373.
[31] N.Q. Vo, R.S. Averback, P. Bellon, S. Odunuga and A. Caro, Phys. Rev. B – Condens. Matter Mater. Phys. 77 (2008) pp.1–9.
[32] N.A. Fleck, G.M. Muller, M.F. Ashby and J.W. Hutchinson, Acta Metall. Mater. 42 (1994) pp.475–487.
[33] Z.H. Aitken, H. Fan, J.A. El-Awady and J.R. Greer, J. Mech. Phys. Solids 76 (2015) pp.208–223.